International Journal of Disaster Risk Reduction 133 (2026) 105979

Contents lists available at ScienceDirect

International Journal of Disaster Risk Reduction

journal homepage: www.elsevier.com/locate/ijdrr

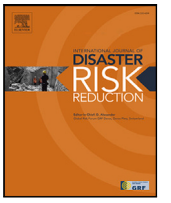

Advancing Earth Observation-based methods for rapid mapping and estimation of flood and drought impacts on rice production in the Philippines

Arnan B. Araza [a,b,*], Elmer Alosnos [c]

[a] Earth Systems and Global Change, Wageningen University and Research, The Netherlands
[b] IMPACT R&D, 47 Razburg, San Agustin Bay, Laguna, Philippines
[c] Philippine Rice Research Institute, Science City of Muñoz, Nueva Ecija, Philippines

ARTICLE INFO

Keywords:
Loss & Damage
Earth Observation
Flood Depth
Agricultural Drought
DRRM
Philippines

ABSTRACT

Floods and droughts increasingly threaten rice production in the Philippines, yet loss and damage (L&D) estimates for rice production are constrained by traditional administrative reporting. While flood and drought extents can be rapidly derived from Earth Observation (EO) data; hazard severity, such as flood inundation depth and extreme drought intensity, remains more difficult to map in near real-time at large scales. This study accounted for the probabilistic nature of hazard severity and integrated it with crop phenology when applying specific damage curves. Rice production costs and baseline yields were subsequently incorporated to quantify disaster L&D from field to administrative levels. Both flooding associated with Typhoon Odette (Rai) and the 2024 drought in Iloilo Province were used as case studies. We estimate that the typhoon damaged 9.3% of rice area and caused losses due to flooding of PHP 270.9 ± 0.8 million, while the 2024 drought damaged 37.6% of rice area with losses of PHP 390.0 ± 0.3 million. Both estimates are lower than provincial reports (flood: PHP 692 million; drought: PHP 707 million). Influencing our estimates is the fact that 59% of rice was at the seedling stage and inundated by only <0.5 m, while during the drought, 85% of rice areas were classified as not highly severe. Moreover, municipality reports may have included unaffected and unverified areas on top of standardized costing practices used. Relative to Typhoon Odette, losses under an extreme flood event (with 1% annual probability) are projected to be up to 3.5 times higher. Hotspots of combined extreme drought and flood events are derived to further support transitions toward impact-based forecasting systems embedded in climate information service platforms.

1. Introduction

Rising sea surface temperatures and increased atmospheric water vapor are driving more frequent and intense hydrometeorological hazards across the Western Pacific, including tropical cyclones, flooding and droughts [1]. This escalation is particularly evident in the Philippines, being consistently ranked first in the Global Climate Risk Index reports [2]. The country faces around 20 typhoons each year and recurrent El Niño events that trigger agricultural droughts, all compounded by limited adaptive and coping capacities [3]. The economic toll is severe particularly in the agriculture sector. The Philippine Statistics Authority (PSA)

* Corresponding author at: Earth Systems and Global Change, Wageningen University and Research, The Netherlands.
E-mail address: arnan.araza@wur.nl (A.B. Araza).

https://doi.org/10.1016/j.ijdrr.2025.105979
Received 1 July 2025; Received in revised form 31 October 2025; Accepted 17 December 2025
Available online 29 December 2025

reported approximately USD 300 million in disaster-related losses between 2012 and 2022 [4]. While national policies on disaster risk reduction and management (DRRM) including post-disaster loss and damage (L&D) are in place, they remain poorly connected to broader development policies and lack comprehensive coverage for the agricultural sector [5].

The Philippine rice sector ranks among the most vulnerable to natural disasters. Grown mainly in lowland areas, rice covers about 3 million ha and provides 34% of the national calorie intake. This vulnerability is intensified by the prevalence of smallholder farmers with 57% cultivate less than 1 ha along with limited resources, which put entire season production costs at risk [6]. Agricultural losses to extreme weather events since the past decade have reached record-high damages [7]. The most devastating event was Super Typhoon Haiyan in 2013, which caused approximately PHP 10.6 billion in agricultural damage, of which 26% was attributed to rice production [8]. Another example is from Typhoon Ursula in 2019, which led to 35–70% yield deficits and extended recovery period for Western Visayas' rainfed farmers [9]. Similarly, recurring agricultural droughts induced by El Niño are also incurring significant damages. For instance, the 2019 El Niño event caused PhP 1.33 billion in crop damage [10]. Flood and drought impacts are further exacerbated by the fact that only around 11% of farmers hold formal insurance, and not all affected farmers receive adequate relief. As of 2017, only about 1.7 million of 8.8 million registered smallholders (19%) are insured [11]. This is compounded by insufficient DRRM funds, which are frequently delayed or difficult to release due to untimely L&D information. Current L&D reporting mechanisms typically rely on coarse, aggregated data and simplifying assumptions during administrative consolidation, which can limit the timeliness and consistency of L&D estimates [4]. The process not only slows the release of farmer insurances and local government calamity funds, but also increases risk to misallocate resources, leaving out the most affected farming communities. Moreover, reliance on manual and incentive-driven reporting can inflate figures in some cases while overlooking localized impacts in others, undermining both transparency and trust in the system [12]. These highlights the urgent need for rapid and accurate L&D appraisal to facilitate timely public relief and recovery efforts.

Earth Observation (EO) offers a solution by providing timely and spatially extensive information on damaged areas, particularly over rice cultivation areas. For instance, Mata et al. [13] used Synthetic Aperture Radar (SAR) data from Sentinel-1 processed in Google Earth Engine to map the flood inundation footprint of Typhoon Ulysses (2020) achieving an accuracy of 95%. The study confirmed that croplands were indeed severely affected while estimating associated losses with the help of local experts. Similarly, Tumaneng et al. [14] demonstrated the utility of SAR data for rapid flood mapping and damage assessment, specifically analyzing agricultural losses from Typhoons Rolly and Ulysses by incorporating localized land cover maps and population density. For drought monitoring, indices derived from optical satellite data, such as the Vegetation Health Index (VHI) from MODIS, have shown potential in indicating agricultural drought severity and damaged areas [15]. This study also indicated yield losses% before and after drought events. The FAO's Agricultural Stress Index System (ASIS) also utilizes VHI to monitor agricultural drought globally and at country-level. For the Philippines, ASIS has been implemented since 2016 to provide crucial 10-day assessments of agricultural drought [16]. There were studies also that used MODIS-based models to estimate crop yields under drought for crop insurance [17,18].

While Mata et al. [13]; Tumaneng et al. [14]; Dumalag et al. [19]; Perez et al. [15] integrated various satellite data sources to enhance agricultural damage monitoring, few have utilized EO data to estimate rice yield L&D itself and yet has to estimate L&D until farm-level. Most applications remain at coarse administrative scales, often provincial or regional, limiting their utility to such scales which is the frontline of disaster response in the Philippines [20]. Farm-level estimates offer clear advantages as they allow more precise targeting of assistance and insurances especially for smallholder farmers. Aside from the scale, it is important to consider the crop phenology which critically modulates vulnerability during specific growth stages of rice [21]. For instance, Boschetti et al. [22] integrated SAR and MODIS to delineate flood extent and assess exposure across different rice stages, however, L&D were not quantified. Kurihara et al. [23] estimated typhoon-induced damage in rice areas but assumed that all rice was at the mature stage. Similarly, although VHI has been used for monitoring agricultural drought per municipality, the use of such index into stage-specific rice yield L&D estimation remains unexplored.

Furthermore, most damage estimates from past studies were reported as deterministic values i.e., without confidence intervals. Consequently, uncertainty in both input data and damage parameters remains unquantified, reducing the reliability of these assessments. Major sources of uncertainty such as classification errors in flood extent maps [24], variability in per-hectare production costs, and the probabilistic nature of the hazard severity itself are seldom accounted for in the final loss estimation. As cautioned by Lagmay and Racoma [25], deterministic maps such as traditional flood susceptibility maps can be misleading, as they fail to capture the range of possible outcomes. In contrast, probabilistic approaches offer a more realistic representation of hazard uncertainty, especially when such estimates serve as basis for government calamity funds or international aid. A robust approach involves using Monte Carlo simulations technique to propagate and combine uncertainties from key input data used to estimate total damages at aggregated levels [26,27].

As current studies are constrained by the L&D estimation at coarse administrative scales, limited consideration of hazard severity and crop growth stages, and the use of deterministic estimates that overlook uncertainty, this study aims to address these gaps by leveraging the increasing EO products on rice crop yield, growth stage, flood and drought together with an uncertainty estimation step in Philippine rice areas. This study applied this framework to two events that affected Iloilo province: the flood impacts of Typhoon Odette (2021) and the 2024 drought event. The L&D estimation and analysis is extended considering a worst-case flood event for comparison and anticipation. Specifically, we aim to (1) Conduct farm-level % yield loss mapping for both flood and drought events that accounts for the probabilistic nature of hazard severity and damage variability depending on crop stages; (2) Compare this EO-derived damage estimates against official government damage reports at municipal to provincial level; (3) Propagate and quantify uncertainty of estimated yield losss using Monte Carlo; and (4) Provide L&D estimates from an extreme flood event. In line with these, we are aiming to answer these research questions:

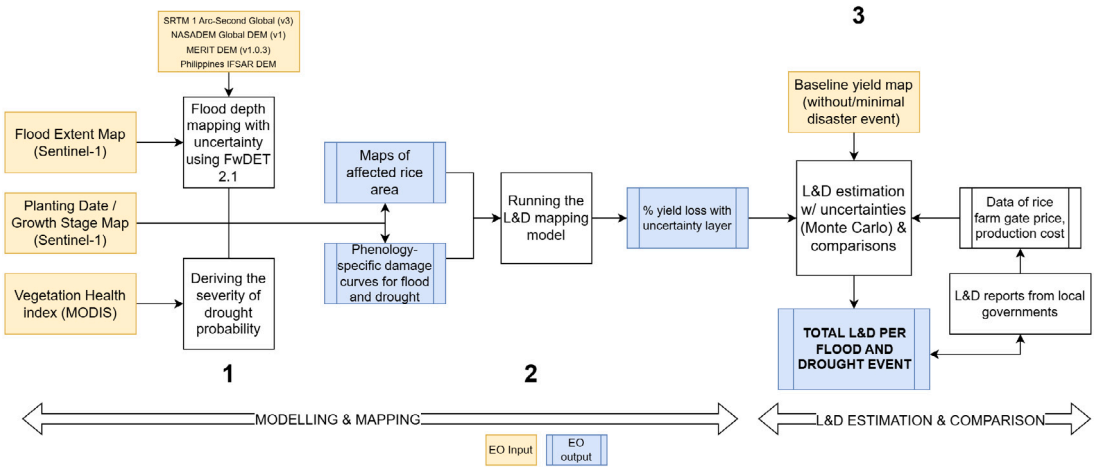

Fig. 1. Overall workflow of the methodology. Highlighted in yellow are EO inputs while blue are EO outputs.

1. How can EO data, integrated with crop phenology and hazard severity (flood and drought), be used to generate estimates of rice production losses from farm to provincial scales?
2. How do these L&D estimates compare with official damage reports from municipalities and even with a worst-case flood event?

2. Materials and methods

Fig. 1 summarizes the methodology workflow of the study and presents the main sections involving the EO inputs and steps used for mapping % yield losses to the L&D estimation proper. The first part is about the flood and drought severity maps; the second part involves running damage model and mapping % damage maps; and the third is the L&D estimation and comparison with local government reports. The diagram shows steps as squares and inputs and outputs as rectangles (yellow if EO input and blue if output), including those with margins as intermediate outputs. We follow the Post-Disaster Needs Assessment (PDNA) definition that damage is the destruction of agricultural assets valued at repair or replacement cost at pre-disaster prices, while losses are the shortfalls in production and income plus added costs until recovery. L&D refers to both physical and monetary estimates, we refer to agricultural drought when we say “drought”.

2.1. Study area

Iloilo Province in Western Visayas (10.7–11.5° N, 122.0–123.6° E) spans approximately 4720 km^2, about 56% of which is classified as agricultural land. The province is a major rice-producing area, with irrigated lowland rice systems dominating the floodplain areas. Based on the Iloilo Provincial Annual Profile [28], the province has a population of roughly 2.56 million, including the highly urbanized Iloilo City. The province receives more than 2000 mm of annual rainfall, concentrated from June to October. The province receives more than 2000 mm of annual rainfall, largely concentrated between June and October. Iloilo is classified as having a high tropical cyclone hazard, and is also prone to El Niño–induced droughts occurring approximately every 3 to 5 years. The western region is bounded by the Central Panay Mountain Range, while the central and eastern lowlands host expansive rice production supported by large-scale irrigation systems. In terms of socio-economic conditions, the province reflects a mix of urban growth and an agriculture-dependent rural economy. While some areas are transitioning to high-value crops and mixed farming systems, rice continues to be the primary livelihood for most farming communities. This combination of topography, climate exposure and agricultural dependence makes Iloilo a strategic case for mapping and managing multi-hazard risks to agriculture under climate change scenarios. See Fig. 2 for the study area map.

2.2. Local government disaster reports

In the Philippines, Local Government Units (LGUs) are mandated to submit post-disaster damage reports within days of a hazard event, detailing impacts on infrastructure, agriculture and livelihoods. These reports are consolidated at the municipal and city levels, then forwarded to the Provincial Disaster Risk Reduction and Management Office (PDRRMO), which collates municipal-wide damage statistics eventually submitted to the region. Coordination is done with national agencies such as the Department of Agriculture (DA) to ensure standard reporting formats and cost assumptions [29,30]. In this study, we used municipal-level reports for Typhoon Rai herein called as Typhoon Odette (local name) and the 2024 drought as reference for comparison with EO-derived estimates.

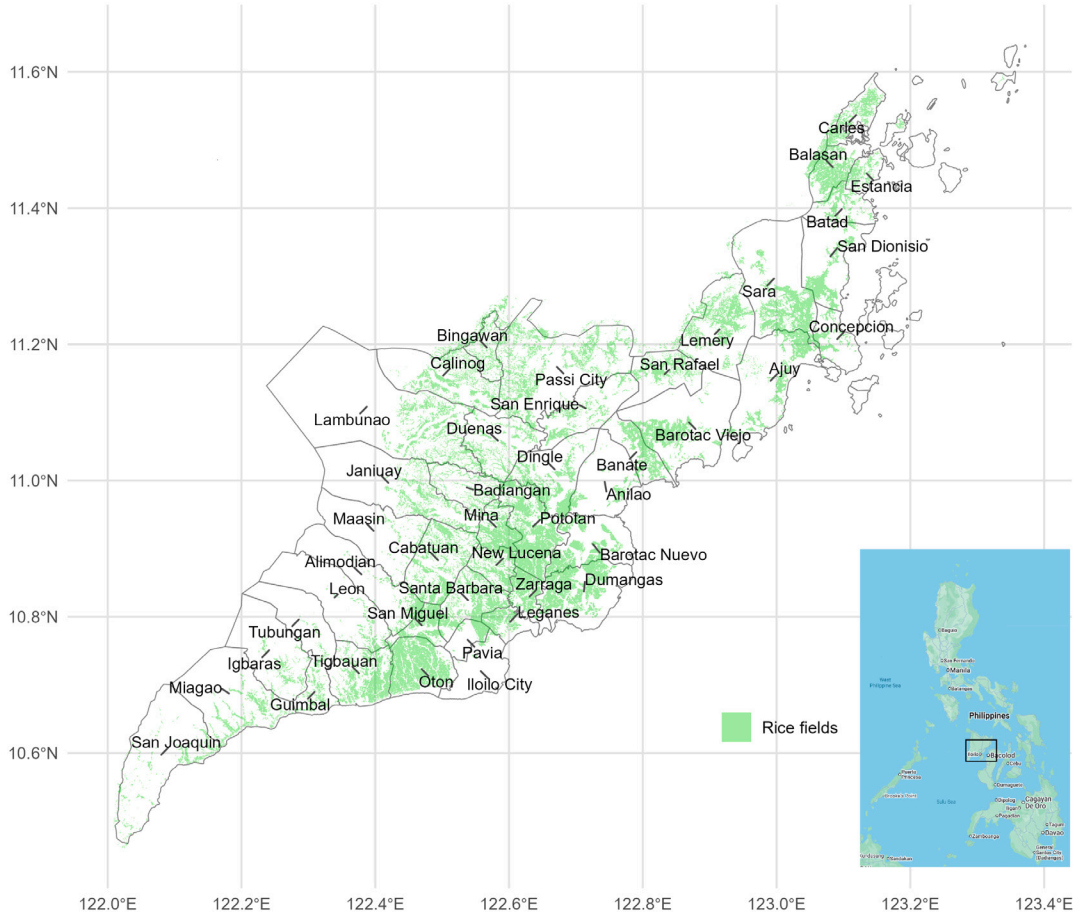

Fig. 2. Study area map of Iloilo province showing recent rice area map (green pixels) from PRiSM data of DA-PhilRice.

Table 1
Input data layers, sources and key references.

Category	Source	Spatial res.	Temporal res.	Main uncertainty	Reference
Rice yield	Sentinel-1, PRiSM	20 m	seasonal	model error	Mabalay et al. [31]
Rice planting date	Sentinel-1, PRiSM	20 m	seasonal	model error	Mabalay et al. [31]
Flood extent	DOST-ASTI	10 m	event	classification error	https://bit.ly/3ywNazl
Flood depth	FWDET v2.1	30 m	event	DEM variability	Cohen et al. [32]
Agricultural drought	MODIS-VHI	1 km	monthly	severity-class thresholds	Bokusheva et al. [33]
Baseline yield	Sentinel-1, PRiSM	20 m	seasonal	model error	Mabalay et al. [31]
Price & production cost	Regional DRR report	n/a	event	sampling and subjectivity	DA,DRRM,LGU 2022–2024
Flood-damage curves	Literature	20 m	static	curve-fit covariance	Kurihara et al. [23]

2.3. Data and preprocessing

Table 1 summarizes the EO data and ancillary datasets, data source and remote sensing data used i.e., mostly based on Sentinel-1. The temporal resolution is also shown with EO products produced during disaster events and rice cropping season. The main uncertainty source of each EO data is also emphasized. All EO data were projected to EPSG:4326 and resampled to 10 m.

2.4. Mapping the flood and drought affected areas

Flood depth mapping using FwDET 2.1

Flood depth was derived with the Flood-water Depth Estimation Tool (FwDET v2.1; Cohen et al. [32]) whose required inputs are a flood inundation mask and a digital elevation model (DEM). The flood inundation mask was obtained from open-access data provided by DOST-ASTI [34]. They used a deep learning classification model using a pair of Sentinel-1 GRD scenes for classifying flood extents e.g., pre-event 2021-12-13 and peak 2021-12-16, VV polarization. The FwDET topography requirement was represented

by a DEM we produced after averaging multiple DEM sources namely SRTM 1″, NASADEM 1″, MERIT 90 m, 5 m IfSAR data and the GEDTM30 v1.1 (see Table S1 for details of the DEM used). The FwDET approach estimated flood depth by converting the flood extent into boundary cells derived from the DEM. The boundary elevations were propagated from the flood boundary toward the interior of the inundated area, assigning each inundated grid cell the elevation of its nearest flood boundary. Flood depth was then computed as shown in Eq. 1.

$$D_i = W_i - Z_i, \tag{1}$$

where D_i is the flood depth at grid cell i, W_i is the estimated water surface elevation and Z_i is the DEM elevation. Uncertainty in flood depth arises from vertical errors in the DEM at both the inundated cell and its associated boundary cell. These uncertainties were propagated to obtain a grid-cell-specific depth uncertainty and flood depth was subsequently represented as a probabilistic variable sampled within the Monte Carlo loss model (Section 2.6).

Probabilistic agricultural drought severity mapping

We derived agricultural drought severity using the Vegetation Health Index (VHI) computed from MODIS NDVI (MOD13Q1; 250 m, 16-day) and daytime land surface temperature (LST; MOD11A1; 1 km, daily), following Kogan [35]. The LST was resampled to 250 m and both variables were aggregated to 14-day composites. VHI was expressed on a 0–100 scale (Eq. 2).

$$\mathrm{VHI} = 0.5\left(1 - \frac{\mathrm{NDVI} - \mathrm{NDVI}_{\min}}{\mathrm{NDVI}_{\max} - \mathrm{NDVI}_{\min}}\right) + 0.5\left(1 - \frac{\mathrm{LST} - \mathrm{LST}_{\min}}{\mathrm{LST}_{\max} - \mathrm{LST}_{\min}}\right) \times 100 \tag{2}$$

Pixel-wise mean VHI was computed over the drought window (January–May 2024) and converted to a normalized drought severity index $S \in [0, 1]$, with higher values indicating more severe stress (Eq. 3).

$$S = \frac{100 - \bar{\mathrm{VHI}}}{100} \tag{3}$$

Thresholds for severe drought reported in the literature vary within the range $S \geq 0.60$–0.70 [15,35,36]. We therefore treated the severity threshold as uncertain within this range and constructed an ensemble of severity masks. The empirical probability of severe drought (p_s) was defined as the fraction of thresholds within this range exceeded at each pixel in (Eq. 4).:

$$p_s = \frac{1}{K}\sum_{k=1}^{K} \mathbb{I}(S \geq \theta_k), \tag{4}$$

where $\theta_k \in [0.60, 0.70]$ denotes severity thresholds sampled within the literature-reported range, K is the number of thresholds considered, and $\mathbb{I}(\cdot)$ is the indicator function. An 80% one-sided confidence criterion was subsequently applied to p_s to retain only pixels with robust evidence of severe drought, yielding both a probabilistic drought severity surface and a confidence-filtered mask suitable for subsequent loss estimation.

2.5. Pixel–level % yield loss mapping

From the rice planting date map, we derived associated crop stages such as seedling, tillering, panicle initiation, heading, milk, soft dough and maturity. They were also grouped into 3 phenological classes: vegetative, reproductive, maturity. Then, for every inundated pixel, the mean water depth and flood duration were discretized to the bins used from data implemented in the Philippines [37] (depth 0-2 m; duration 4, 8, 12, 16, 20 or ≥27 days). These three inputs consist the depth-duration-stage matrix and damage curve [37] and written to a raster of % yield loss. The matrix gives integer values, so the resulting map represents a mean loss.

The same procedure was applied to drought-affected pixels, replacing flood depth with drought severity map. The VHI composites for January–May 2024 were first converted to a pixel-wise probability of "severe" stress, p_s, by evaluating thresholds from 30–40% severity. The mean probability therefore embodies the disagreement among sources, while the variance $\sigma_s^2 = p_s(1-p_s)$ quantifies that ambiguity. For each crop stage the corresponding minimum and maximum drought losses were linearly interpolated with weight p_s, producing an expected drought-loss raster L_d and an accompanying uncertainty $\sigma_{L_d} \propto \sqrt{p_s(1-p_s)}$. Flood loss L_f is thus controlled by discretized depth–duration classes, whereas drought loss L_d is modulated by probabilistic VHI severity.

2.6. Loss estimation and comparisons

Loss estimation from pixel to aggregated levels.

The losses were estimated by integrating two monetary components: (i) revenue losses due to reduced paddy yield and (ii) production costs already incurred by farmers at the time of the event. Revenue loss was computed by combining the baseline yield without or minimal disaster event (see Table 1), the % yield loss and farm-gate prices sampled from the empirical price distribution observed during the two-week post-event trading window. This valuation follows the framework commonly used in DA and LGU calamity assessments.

Uncertainty in hazard severity, yield loss, prices and production costs was propagated using a Monte Carlo simulation framework implemented at the pixel level. For each grid cell, multiple realizations were generated by repeatedly sampling stochastic inputs,

including flood depth uncertainty, probabilistic drought severity, price variability, and cost variability. In each realization, pixel-level damage cost was computed only for cells classified as affected, thereby accounting for commission errors in flood mapping and uncertainty in drought masking.

For each Monte Carlo realization, pixel-level monetary damage was estimated according to Eq. 5:

$$D^{(n)} = Y_0\, L^{(n)}\, P^{(n)} + C^{(n)}, \tag{5}$$

where Y_0 is the disaster-free baseline yield, $L^{(n)}$ is the sampled fractional yield loss, $P^{(n)}$ is the farm-gate price drawn from the empirical price distribution, and $C^{(n)}$ is the production cost sampled from the province-specific cost distribution.

The ensemble of Monte Carlo realizations yielded pixel-wise distributions of monetary loss, from which the mean expected damage and associated uncertainty were derived. These pixel-level estimates were then aggregated to administrative levels using area-weighted summation. Province-level expected loss and uncertainty were computed following Eq. 6:

$$\mu_{\text{tot}} = \sum_{i \in \mathcal{A}} A_i\, \mu_{D,i}, \qquad \sigma^2_{\text{tot}} = \sum_{i \in \mathcal{A}} A_i^2\, \sigma^2_{D,i}, \tag{6}$$

where $\mathcal{A}$ denotes the set of pixels within the administrative unit, A_i is the pixel area, and $\mu_{D,i}$ and $\sigma_{D,i}$ are the mean and standard deviation of pixel-level damage derived from the Monte Carlo ensemble, assuming spatial independence of errors. Reported loss and damage estimates were presented as expected values with corresponding 95% confidence intervals.

Comparison of estimates with local reports and extreme events

At the municipality level, we compared the L&D estimates from this study and the local reports (Sect. 2.2) through scatterplots and mirroring bar graphs. We estimated the Pearson's correlation *(r)* among the two sources while paying attention to the magnitude of disagreement. We further compared the spatial pattern and magnitude of losses by highlighting whether the LGU-based is higher than 20% than EO-based and vice versa.

Another set of comparisons was initiated between Typhoon Odette (2021) and extreme flood event i.e., a flood with a 1% annual probability of occurrence Lagmay [38]. We summed per-pixel loss estimates for Typhoon Odette and the extreme flood scenario, then computed both million-PHP to allow direct comparison. We assessed agreement in flood hotspots by computing the overlap of binary flood extents and by calculating the correlation between municipality-level loss totals.

For agricultural drought, we applied an empirical threshold of VHI $\leqslant$ (mean=0.2) to derive an expanded drought-extent mask, which was clipped to the rice-growing area. We then overlaid the binary maps for the extreme flood scenario and the expanded drought extent to identify multi-hazard "hotspots" and summarized both the absolute hotspot area (ha) and its share of total rice area by municipality.

3. Results

3.1. EO inputs and the spatial yield loss map

Fig. 3 shows the map inputs used to estimate the pixel-level and total rice production losses due to flooding from Typhoon Odette in mid-December 2021. The majority of the rice area then was in the seedling stage (59.2%), followed by tillering (21.5%) and panicle initiation (8.2%). In terms of spatial patterns, the most low-lying paddies in north-eastern and south-western Iloilo were still in the panicle-initiation or booting stage, whereas most of the mainlands were already at transplant and tillering. Because the depth–duration damage curve penalizes later stages more, the spatial pattern in crop stage depicts where large yield losses are possible. Baseline yield (t ha^{-1}) (from the cropping season without or with minimal disaster event) confirms this as yields can exceed 4 t ha^{-1} along the western area but drop below 3 t ha^{-1} in fragmented areas in the northern part. Flood depth (m) indicates that inundation reached 1.5–2 m while most of the rice domain remains dry (<0.5 m). The Flood-depth uncertainty σ (m) is largely <0.25 m and these coincide with areas with deeper inundation. The % yield loss converts depth, duration and crop stage into expected fractional loss. Damaged areas ($\geqslant$ 60%) appear over the deepest water in central Iloilo where crops were at sensitive reproductive stages, while peripheral paddies show only the minimum 40% prescribed by the damage curve. The % yield loss uncertainty mirrors yield loss spatial patterns but peaks where both the depth error and the curve's slope are large. Overall, around 9.3% of the rice areas were inundated based on the flood extent map and the total rice area derived from the crop stage map.

Fig. 4 presents the EO layers used to derive the 2024 dry season drought-yield loss calculation. The crop-stage maps reveal that, by early April, nearly the entire rice fields had advanced to dough or maturity and only several areas remained at booting and milking. The drought-damage table assigns its lowest sensitivity to these late stages, the stage alone suggests that potential yield loss can be moderate. The maturity stage occupied the majority of the cropped area (72.8%), with relatively low and stable damage (mean 15%), see Table S3. This is reinforced by the baseline-yield map whose values peak at 5 t ha^{-1}. When severity is merged with the stage-specific drought curve, the resulting yield loss % map indicates losses of roughly 14%–18% concentrated in the same agricultural drought hotspots. Elsewhere, the predicted loss defaults to the damage curve's stage minimum of 14%. The yield-loss uncertainty (σ) is mostly under 5%, rising to 10%–15% where VHI ambiguity coincides with steep damage curves. Around 37.6% of the rice areas had severe agricultural drought based on the severity index map and the total rice area derived from the crop stage map.

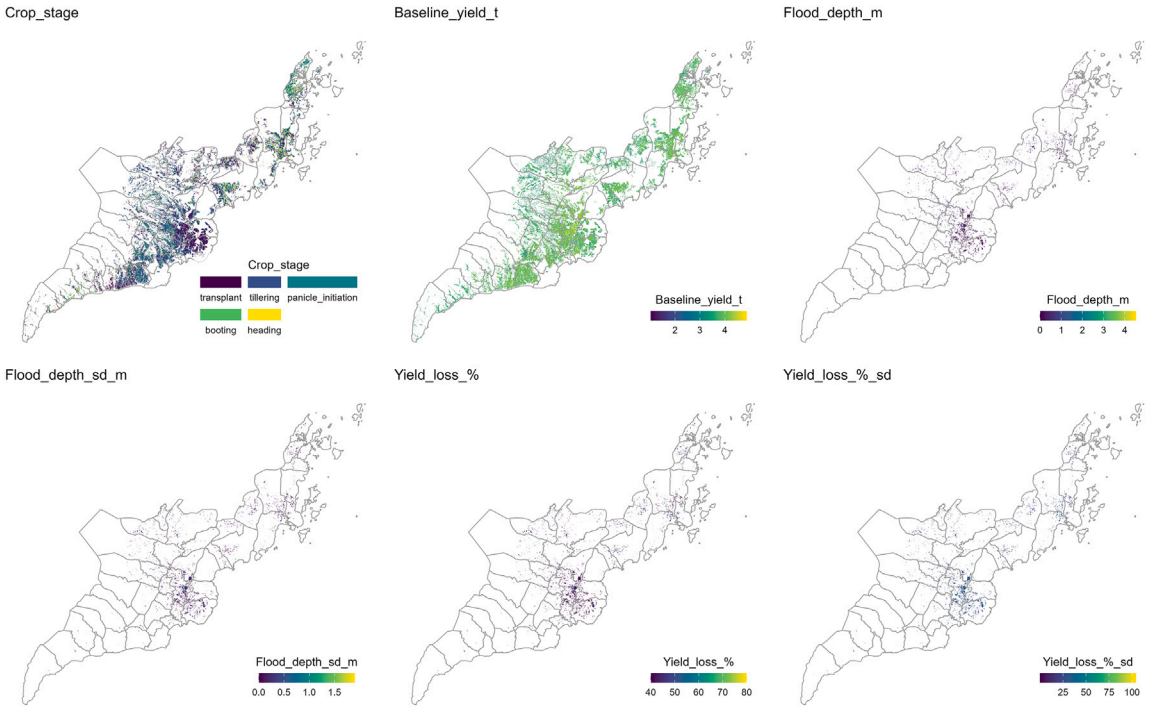

Fig. 3. Map inputs used to derive the spatial rice production losses (PHP) from the Typhoon Odette event.

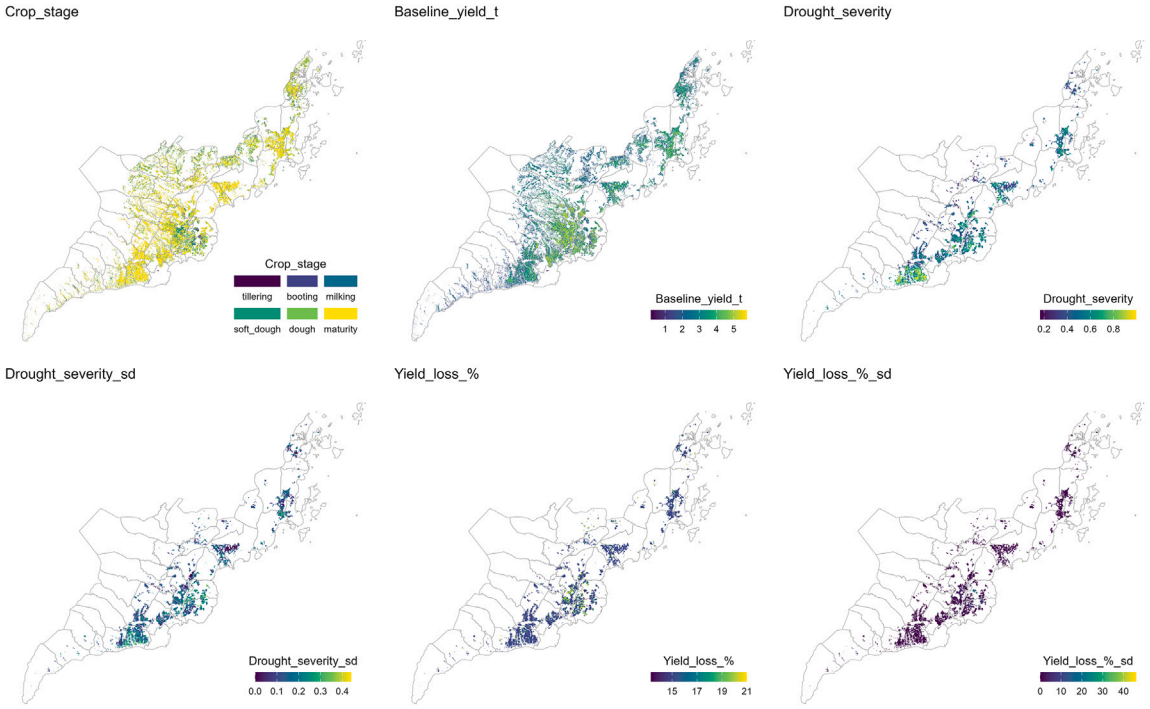

Fig. 4. Map inputs used to derive the spatial rice production losses (PHP) from the 2024 drought event. Note that color scaling and bins differ from Fig. 3.

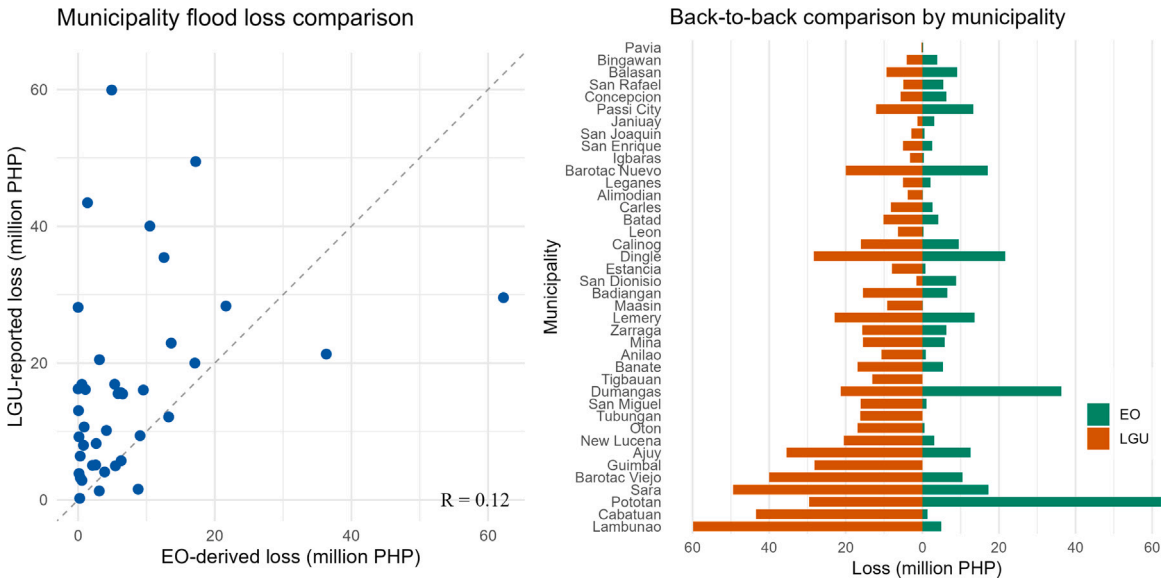

Fig. 5. Comparison between the EO-derived and national reports total losses (PHP) of a flood event at municipality level.

3.2. Comparison of our estimates with the local reports

Fig. 5 shows that EO-based loss estimates are generally lower than the values reported by municipalities. Most points are found above the 1:1 line and the coefficient of determination is modest (*r=0.12*), indicating limited alignment between the two sources. The bar graph confirm that, for the majority of municipalities, reported losses way exceed those derived from this study, while only a few localities (e.g. Pototan and Dumangas) display the reverse pattern. The two are located in the central part of the province, see Fig. 2. There are at least 7 municipalities that showed good agreement between EO-based and local reports i.e., the topmost municipalities in the comparison figure located in different parts of the province.

Fig. 6 compares EO-derived and municipality-reported drought losses. Agreement is *r=0.21*, yet the scatter is more balanced around the 1:1 line than for the flood case as several municipalities (e.g., Pototan, Dumangas and Barotac Viejo) show larger EO estimates, while others (such as Lambunao or Calinog) report markedly higher figures based on local reports. The figure emphasizes this mixed pattern and reflects the strong local variability in VHI-based drought severity and planting dates, as well as possible differences in how area-based reports accounted for harvests or late crop management.

The spatial interpretation in Fig. 7 shows that most municipalities report losses that differ from EO-based estimates by more than ś20%, with LGU-reported values more frequently exceeding EO-based estimates for both flood and drought events. Discrepancies are spatially heterogeneous, with fewer municipalities falling within the ś20% agreement range. Reporting coverage was lower for the drought event (32 of 44 municipalities; 72%) than for Typhoon Odette (40 municipalities; 90%). Only one municipality reported losses lower than the EO-based estimates for both flood and drought.

3.3. Estimates for an extreme flood scenario

Figs. 8 and 9 present a side-by-side comparison of the Typhoon Odette flood and an extreme flood event. The inundation of the extreme event covers the entire river network and adjacent lowlands, resulting in a much broader and more intense damage pattern and estimate than the flooding from Odette. Municipality level losses follow a linear trend between the two events (*r=0.66*). Interestingly, Odette's flood damage is larger in several municipalities that are considered flood hotspots such as Pototan and Dumangas. The spatial overlap of the two flood events is found to be 64%, while the range of the farm-level damage is PHP 1,000–2,500 per 100 m^2.

3.4. Total damages comparison and hotspot analysis

The EO–based estimates showed lower provincial totals than the locally reported loss figures and with low uncertainty estimates (Table 2). For Typhoon Odette, our estimate is only ~ 271 M PHP, about 2.6 smaller than the 692 M PHP consolidated by the provincial office. A similar, though slightly narrower, gap appears for the 2024 drought (390 M PHP from EO versus 707 M PHP reported, a factor of ~ 1.8). Within the EO results the 2024 drought caused ~ 1.4 more monetary loss than the Odette flood (390 M PHP vs 271 M PHP). Although drought affected far fewer hectares than the extreme flood extent, its timing coincided with the reproductive phase of a large portion of the crop and the damage curve assigns disproportionately high penalties to water stress at that stage. Provincial total suggests parity between the two estimates (707 M PHP drought vs 692 M PHP flood).

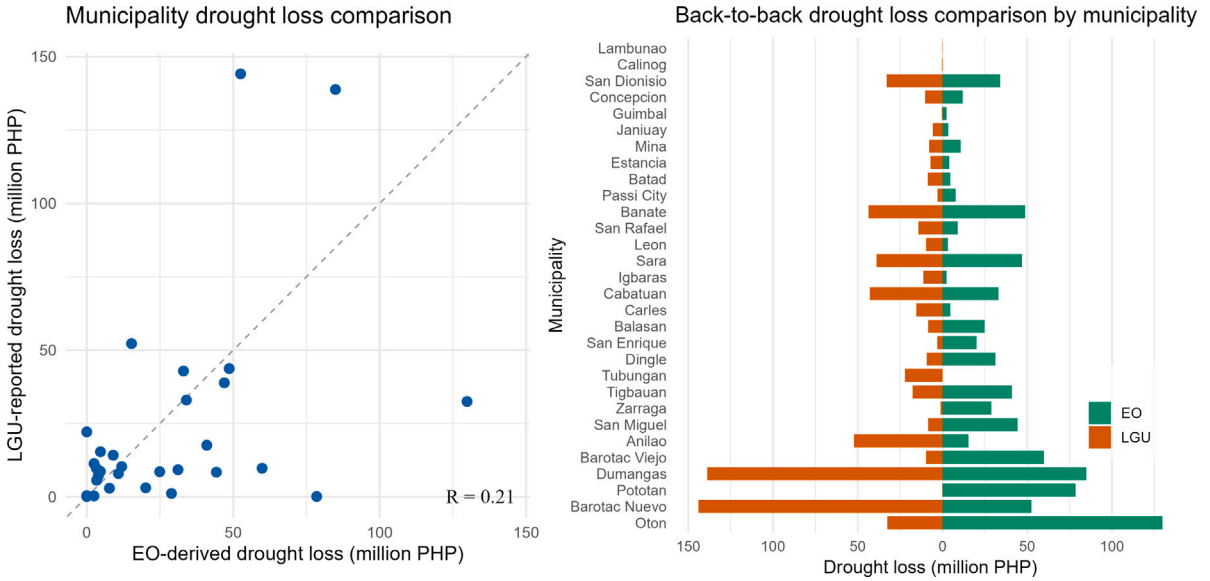

Fig. 6. Comparison between the EO-derived and national reports total losses (PHP) of a drought event at municipality level.

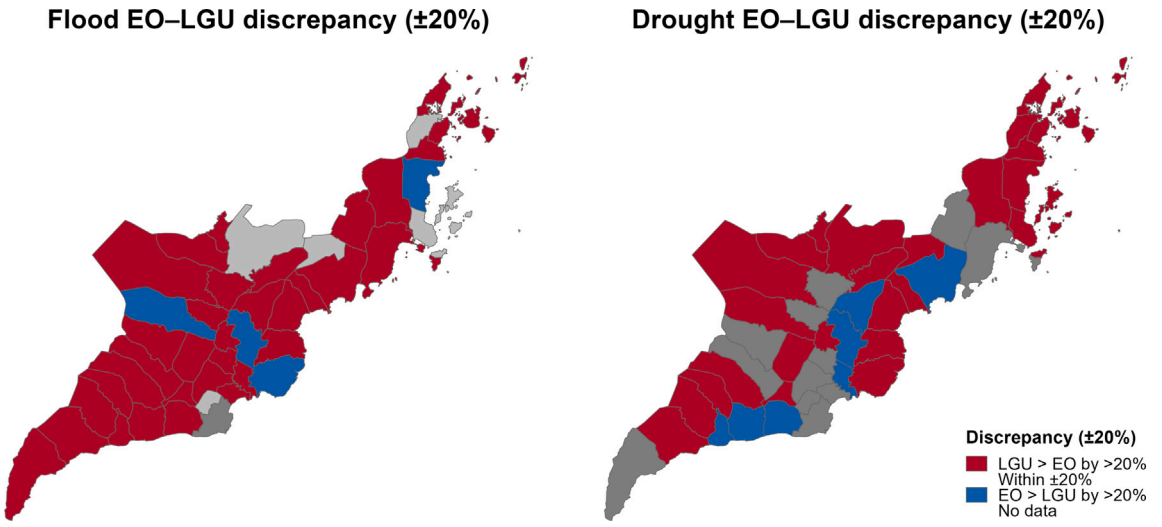

Fig. 7. Maps showing whether municipalities estimated higher or lower than EO-based estimates. Light gray depicts < 20% discrepancy while darker gray means no data.

Table 2
Municipality-level losses (in M PHP) from this EO-based study versus provincial reports and an extreme flood scenario.

Event	This study	Loss (M PHP)	Comparison	Loss (M PHP)
Typhoon Odette Flood	EO-based	270.9 ± 0.8	Provincial report [29]	692.3
2024 Drought	EO-based	390.0 ± 0.3	Provincial report [30]	706.6
Extreme flood event	–	–	1:100-year flood model [38]	1694.2 ± 1.8

The extreme flood scenario delivers a province-wide loss of 1.69 B PHP roughly 3.5 more than the estimates from the Typhoon Odette. The multiplier is driven mostly by extent i.e., the extreme flood inundates almost every areas parallel to stream networks, whereas Odette's footprint was confined to the Jalaur and Iloilo River basins.

The hotspot analysis in Fig. 10 identifies ten municipalities i.e., Pototan, Mina, Balasan, Banate, Oton, Sara, Dumangas, Barotac Viejo, Ajuy and Dingle that each have over 1000 ha of rice lands simultaneously exposed to severe flood and drought hazards. Pototan and Mina are most heavily impacted, with nearly 30% of their total rice area in the multi-hazard hotspot.

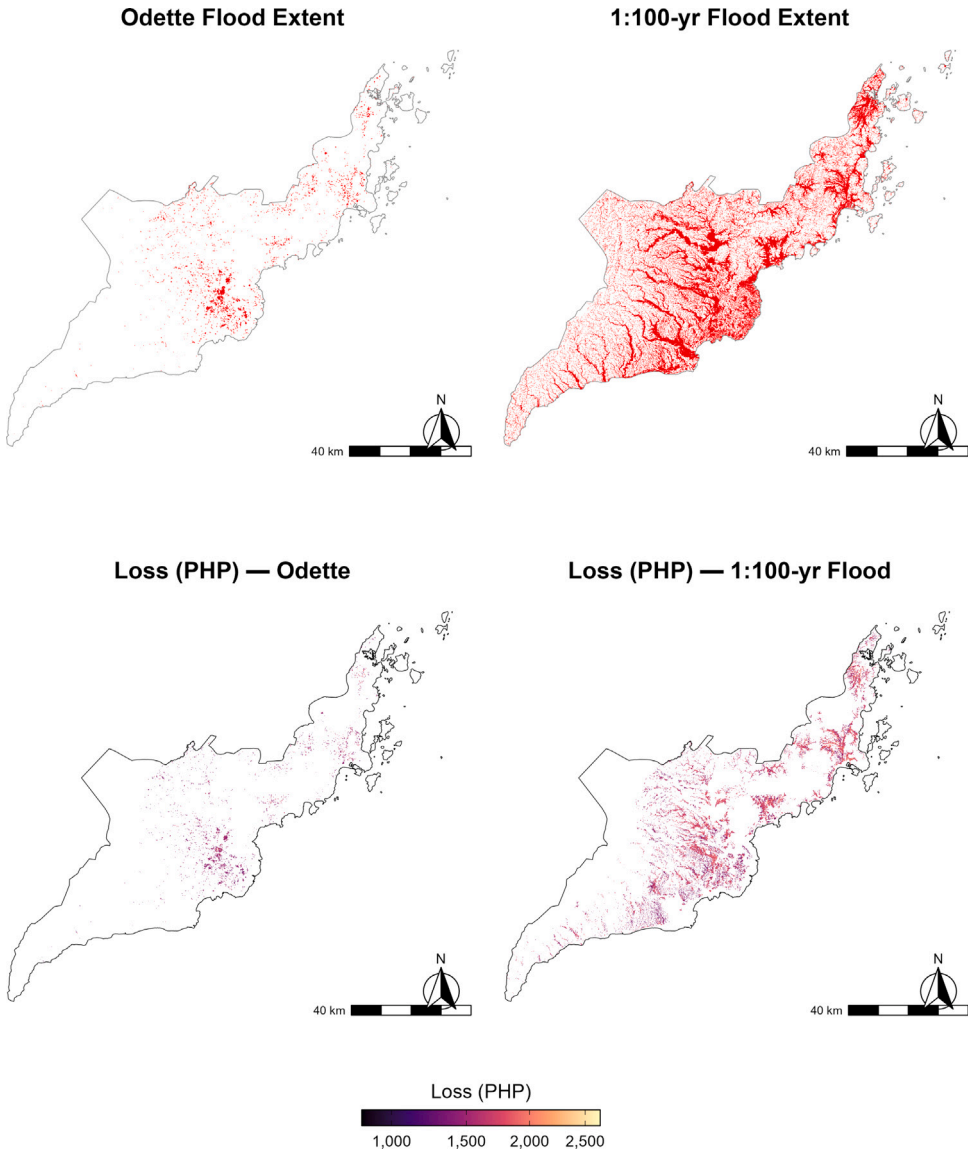

Fig. 8. Comparison between the flood extent maps (10 m) of a Typhoon Odette and an extreme flood event and the associated losses (PHP) at pixel level.

4. Discussion

4.1. Deriving the spatial % yield loss maps

Our spatial analysis demonstrated that crop phenology strongly influences rice yield losses in both the flood event (59% seedling stage) and drought event (73% maturity). Fields in reproductive stages particularly panicle initiation and heading showed disproportionately higher damage under moderate drought or flood stress. This aligns with findings by Shrestha et al. [39], who developed flood vulnerability curves for rice in Myanmar with significant losses during reproductive phases and Boschetti et al. [22] who showed that phenology-aware remote sensing and damage estimation is important for flood damage assessment accuracy. More studies suggest that short-duration flooding during early vegetative stages inflicts substantially less yield loss than similar stress applied during reproductive stages, as early-stage rice can often recover through tillering and vegetative regrowth e.g., Ismail [40]; Yu et al. [41].

Although fewer than 10% of rice-growing areas were inundated and classified as “severely affected” by Typhoon Odette or the 2024 drought when using Vegetation Health Index (VHI) thresholds respectively, these assumptions may also underestimate actual impact. In the 2019 El Niño–induced drought in the Philippines, Perez et al. [15] showed that while VHI and related indices

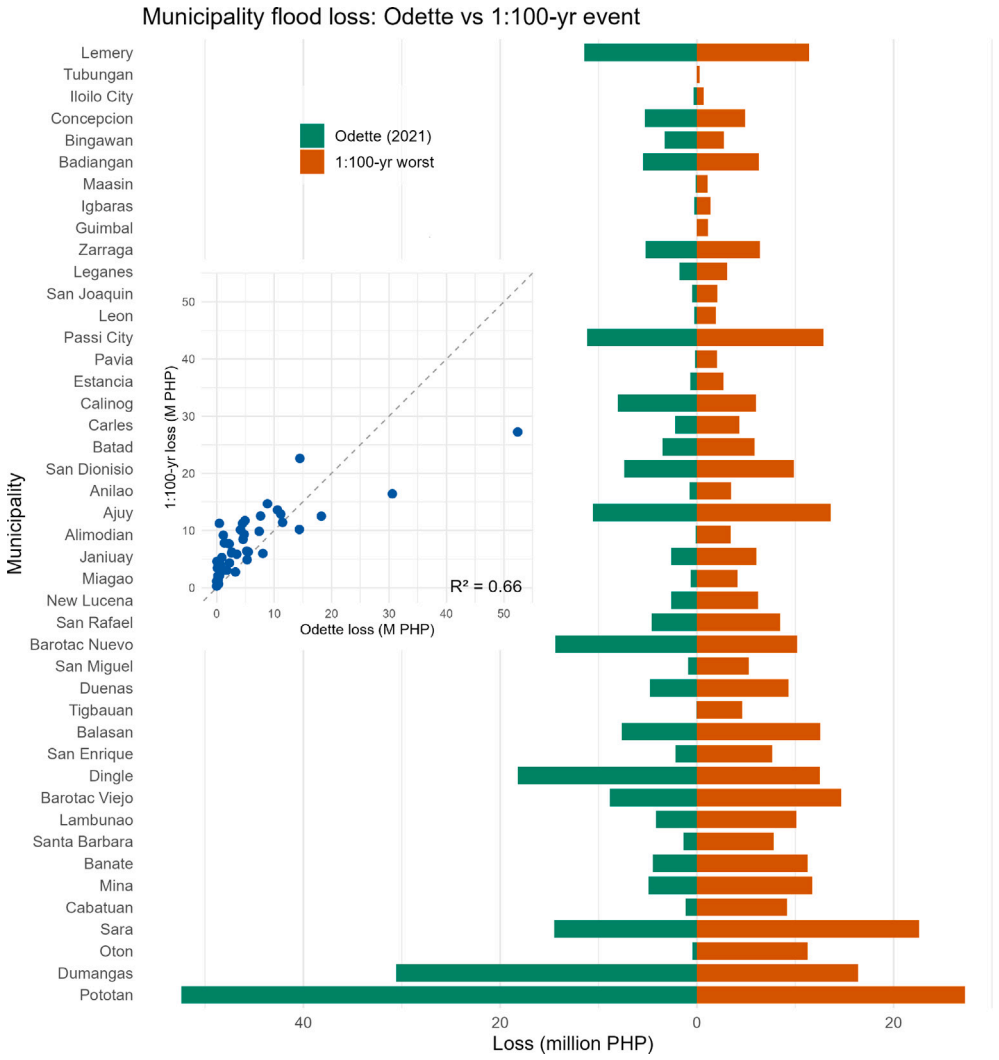

Fig. 9. Comparison (scatter plot and bar graph) between the flood extent maps of a Typhoon Odette and an extreme flood event and the associated damage costs for all municipalities.

classified roughly half of agricultural land as stressed, rice yield losses still reached up to 20% in a western province during the first two quarters following the El Niño peak. Consistent with this pattern, earlier El Niño events in the 1990s were associated with national rice production declines of approximately 6% during moderate events and up to 22% during strong events [42]. These findings highlight that even areas classified under "moderate" or "mild" stress zones can experience substantial yield reductions, demonstrating that using only a strict "severe" threshold can underestimate agronomic loss. For instance, Villa et al. [43] reported that moderately severe drought can still cause 59% damage to crops.

Omission errors in flood extent maps can result in underestimation of affected areas especially when flooding is short-lived or recedes before next pass of Sentinel-1. This repeat cycle (typically 6 to 12 days) often misses transient inundation events especially in tropical areas with brief intense flooding followed by rapid drying. In Luzon, Philippines, an inter-comparison of Sentinel-1 change detection algorithms during a typhoon event revealed that single-date SAR scenes failed to capture several flood pulses, resulting in under-mapping unless multi-date temporal analysis was applied [24]. Similarly, a Bangladesh study reported that rapid flood recession substantially reduced backscatter signals before satellite acquisition, leading to omission of affected areas [44]. On the other hand, commission errors of 5–15% is also possible as fishponds, irrigation canals and saturated fallows often resemble open water in C-band SAR imagery [45]. These false positives may inflate water depth fields derived from terrain-fitting models like FwDET [32].

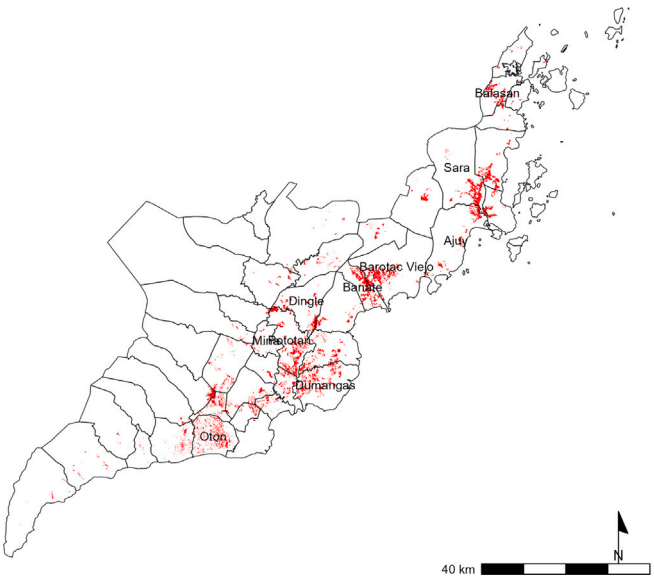

Municipality	hotspot_ha	muni_area_ha	pct_hotspot
Pototan	2777.0	9728.5	28.5
Sara	2113.5	19195.8	11.0
Dumangas	1675.4	12162.0	13.8
Barotac Viejo	1416.7	18864.8	7.5
Balasan	1261.7	5135.1	24.6
Ajuy	1237.1	17047.8	7.3
Oton	1221.1	8578.2	14.2
Mina	1158.0	4032.7	28.7
Banate	1126.7	5202.9	21.7
Dingle	1083.6	10361.4	10.5

Fig. 10. Hotspot areas of a combined extreme agricultural drought scenario and the extreme flood events.

4.2. Comparison of loss estimates: EO-based and municipal reports

We found that the EO-based loss estimates were generally lower than the values reported in municipal summaries. Our results are consistent with van Rutten et al. [45], who demonstrated that using Sentinel-1 flood extent and FABDEM-derived depth values in combination with rice damage curves produced lower loss estimates than ground-based reports. One reason is the interplay of crop stages and hazard severity extent that directly affect recovery [46]. However, the damage curves used can still improve by further accounting other influential factors like rice variety which both incur different recovery properties and production costs [43,47].

The systematic higher estimates from local reports can be plausibly attributed to a combination of methodological and administrative factors. First, local reports may have included unharvested yet ultimately unaffected fields in their initial assessments, particularly when early forecasts were pessimistic and aimed at preemptive relief mobilization. Higuchi et al. [12] reported that administrative damage figures in the Philippines frequently overestimated actual losses when compared with satellite imagery and survey data, suggesting that unaffected areas were systematically incorporated into the damage estimates to secure faster relief disbursements. Second, there appears to be a widespread tendency to apply the highest allowable production-cost rates uniformly, regardless of the actual practices or input levels specific to a locality. Flyvbjerg et al. [48] argued that such behavior is often not due to error but to deliberate misrepresentation to maximize funding eligibility or political gain.

The loss estimates had narrow 95% confidence intervals (±0.8 M PHP for the flood event and ±0.3 M PHP for the drought event), indicating low uncertainty under the current assumptions considering the production costs and yield-loss parameters. Such error propagation can be expanded considering probabilistic nature of other damage model inputs (e.g., remote sensing maps, market price volatility) while checking their spatial dependencies to avoid underestimation of uncertainty [49].

On the other hand, we found that those municipalities that showed good agreement between EO-based and local estimates are located in different parts of the province i.e., no spatial pattern that can be associated with the agreement. Aside from technical capacity, socio-political issues and geophysical conditions may play a role on how effective they can enact DRRM [50].

4.3. Climate change extreme impact and hotspots

The extreme flood scenario analysis revealed an estimated province-wide loss of 1.69 B PHP roughly 3.5 more than the estimates from the Typhoon Odette. We find this surprising as we expected higher estimate from the extreme flood scenario. The extreme flood map comes from a hydrodynamic simulations that restrict flooding to hydraulically connected zones. This modeling approach may reduce commission errors over ambiguous surfaces but may also omit floodwater in hydraulically disconnected rice fields. Recall also that the two flood extent maps only overlaps by 64%. Our comparison with a flood scenario aligns with a vulnerability assessments study that linked flood return periods to stage-specific yield loss [51].

Three high-exposure municipalities (Mina, Balasan and Oton) highlighted the vulnerability to both flooding and drought. These overlapping hotspots should be prioritized in the Provincial DRRM Plan by targeting both structural flood defenses and drought-resilient irrigation and storage in the highest-risk towns in line with the Philippine Disaster Risk Reduction and Management Act of 2010 (RA 10121).

4.4. Implications and future work

While the method and analysis of this study are limited to rice and two major climate hazards, the framework and methodology are replicable and adaptable to other crops and provinces in the Philippines. The findings underscore the need for EO-supported verification mechanisms in the release of calamity funds under RA 10121 to enhance transparency and farmer trust. Mapping phenology-sensitive hotspots provides an evidence base for targeting flood- and drought-tolerant rice varieties (e.g., NSIC Rc 194, Rc 222, Rc 480), water-saving rice technologies (e.g., dry direct seeding, laser land leveling, Alternate Wetting and Drying or AWD) and other climate-smart approaches in high-risk municipalities. EO-based rapid assessments can also underpin index-based insurance and parametric payout schemes to ensure timely and equitable farmer compensation [52].

This study relied on official EO products from national agencies e.g., crop stage maps where delays in release and access may compromise the timeliness of rapid assessments. Such stage-specific damage functions applied are preliminary and can be updated as new empirical data on crop losses become available. In terms of the flood extent dependency, thanks to timely production and sharing of Philippine Space Agency, we already have L&D estimates from recent flood events on July 18 and September 22, 2025, which will be shared and visualized via our WebGIS platform www.digisaka.com (Fig. S1). The mobile application of Digisaka also functions as a ground validation tool.

Looking ahead, our findings highlight the urgent need for an impact-based forecasting system that links real-time hazard mapping with DRR, relief operations and insurance mechanisms for rice farming communities e.g., [53,54]. This will indicate not only where and when floods or droughts will occur, but also how they will affect livelihoods and production, enabling anticipatory actions and risk financing such as index-based insurance [55]. Embedding this within digital agriculture platforms would facilitate transparent, public-facing dashboards that deliver tailored agro-advisories to farmers and local decision-makers [31,38]. Moreover, future flood and drought mapping efforts stand to benefit greatly from ultra-high-resolution UAV images, which can deliver near-real-time inundation extents and depths [56]. For flood mapping, terrain-driven approaches such as the Height Above Nearest Drainage (HAND) model further refine these predictions by integrating catchment topography to estimate likely floodwater depths without requiring full hydrodynamic simulations [57]. Moreover, integrating IoT-enabled river-stage and discharge sensors provides continuous observational data streams that can automatically recalibrate and update flood extents as water levels change [58].

A spatially explicit risk framework should focus on multi-hazard hotspots i.e., areas prone to flooding, drought, wind damage and pest outbreaks so municipal governments can prioritize interventions. These can all have stand-alone and compounded damage curves and matrices estimated from actual updated data. Moreover, a comprehensive L&D accounting system in a WebGIS environment that integrates wind effects, pest and disease stressors, rice varieties, water management and stage-specific yield-loss would support proactive DRR planning and more equitable budget allocation to the most-affected municipalities. In addition, forecasts of rice yield and prices can further inform preparedness and response decisions. We piloted such a platform that also functions as a Climate Information Service (CIS), integrating real-time weather information with crowdsourced inputs (Fig. S1). This platform provides a pathway for delivering near real-time estimates of loss and damage following disaster events. Lastly, this study should complement national government L&D reporting systems, improving efficiency and timeliness in capturing disaster impacts on rice.

5. Conclusion

This study demonstrates that integrating EO-derived hazard maps with hazard severity and crop phenology enables robust estimation of rice production losses beyond what is typically captured in conventional administrative reports. Typhoon Odette affected 9.3% of rice areas with losses of 270.9 ± 0.8 million PHP, while the 2024 drought stressed 37.6% of rice areas with losses of 390 ± 0.3 million PHP, both considerably lower than local government reports. While discrepancies exist, they also underscore the complementary roles of EO-based and ground-based reporting systems, where administrative data provide institutional coverage and EO-based approaches help reveal spatially heterogeneous impacts and severity patterns that may otherwise be missed. Such areas are best to be validated from the ground e.g., crowdsourcing using digital tools. The identified damage hotspots align with multi-hazard regions, underscoring the need for spatially targeted DRR and climate-smart interventions. Looking ahead, operationalizing rapid loss assessment within a Climate Information Service platform such as *Digisaka*, coupled with integration of actual farm-level production costs, will allow pixel-level losses to be expressed in direct economic terms for insurance, calamity funds and farmer compensation. Future work should also develop impact-based forecasting and farmer co-reporting mechanisms to enhance both the timeliness and reliability of disaster assessments.

CRediT authorship contribution statement

Arnan B. Araza: Writing – original draft, Validation, Methodology, Investigation, Formal analysis, Conceptualization. **Elmer Alosnos:** Writing – review & editing, Data curation, Conceptualization.

Ethical statement

All authors have read, understood and have complied as applicable with the statement on "Ethical responsibilities of Authors" as found in the Instructions for Authors.

Funding

This research received no external funding; the study was undertaken in the spirit of public service to the nation.

Declaration of competing interest

The authors declare that they have no known competing financial interests or personal relationships that could have appeared to influence the work reported in this paper.

Acknowledgments

The authors would like to thank the Provincial Government of Iloilo and Department of Agriculture - Regional Field Office VI for sharing the DRR reports used in this study; Department of Science and Technology - Advanced Science and Techonology Institute (DOST-ASTI) for flood maps and the Philippine Space Agency (PhilSA) for subsequent flood maps from other typhoon events; Philippine Rice Information System (PRiSM) Unit of DA-PhilRice for rice area, growth stage and yield maps; and Leads Agri for the innovation and scaling support.

Appendix. Supplementary materials

See Tables S.1–S.3 and Fig. S1.

Table S.1
Gridded data sets used in the flood–depth workflow.

Data set	Brief description	Nominal res.	Reference
SRTM 1″	Space-borne C-band DEM (v. 3, void–filled).	30 m	Farr et al. [59]
NASADEM 1″	SRTM re-processing with ICESat	30 m	Crippen et al. [60]
MERIT DEM	Multi-error-removed global DEM; hydrologically conditioned	90 m	Yamazaki et al. [61]
Phil. IfSAR	Interferometric airborne SAR DEM for the Philippines	5 m	DOST LiDAR Program (2019)
Composite DEM	Error–weighted average of the four DEMs above	30 m	this study
FwDET depth map	Floodwater depth raster for Typhoon Odette (2021); produced with FwDET v2.1	30 m	Ho and Hengl [62]

Table S.2
Area distribution and yield loss statistics by crop stage for the flood event caused by Typhoon Odette.

Stage	Cells	Area (ha)	Mean	Median	Q25	Q75	Min	Max	% Area
Seedling	123,132	4896	42.1	40	40.0	40.0	40.0	72.3	59.2
Tillering	44,797	1781	41.7	40	40.0	40.0	40.0	70.1	21.5
Panicle initiation	17,126	681	41.5	40	40.0	40.0	40.0	69.0	8.23
Heading	12,840	511	59.4	60	58.0	60.0	45.2	80.0	6.17
Booting	10,124	403	42.8	40	40.0	40.0	40.0	74.6	4.87

Table S.3
Area distribution and yield loss statistics by crop stage for the 2024 drought event.

Stage	Cells	Area (ha)	Mean	Median	Q25	Q75	Min	Max	% Area
Maturity	5949	23,653	15.1	15.0	15.0	15.0	13.3	21.0	72.8
Dough	941	3741	15.5	15.0	15.0	15.0	13.3	21.0	11.5
Soft dough	514	2044	17.9	18.7	15.0	20.6	13.3	21.0	6.29
Milking	456	1813	17.6	18.1	15.0	20.0	13.3	21.0	5.58
Booting	209	831	15.5	15.0	13.7	15.7	13.3	21.0	2.56
Tillering	104	414	15.5	15.0	15.0	15.0	13.3	21.0	1.27

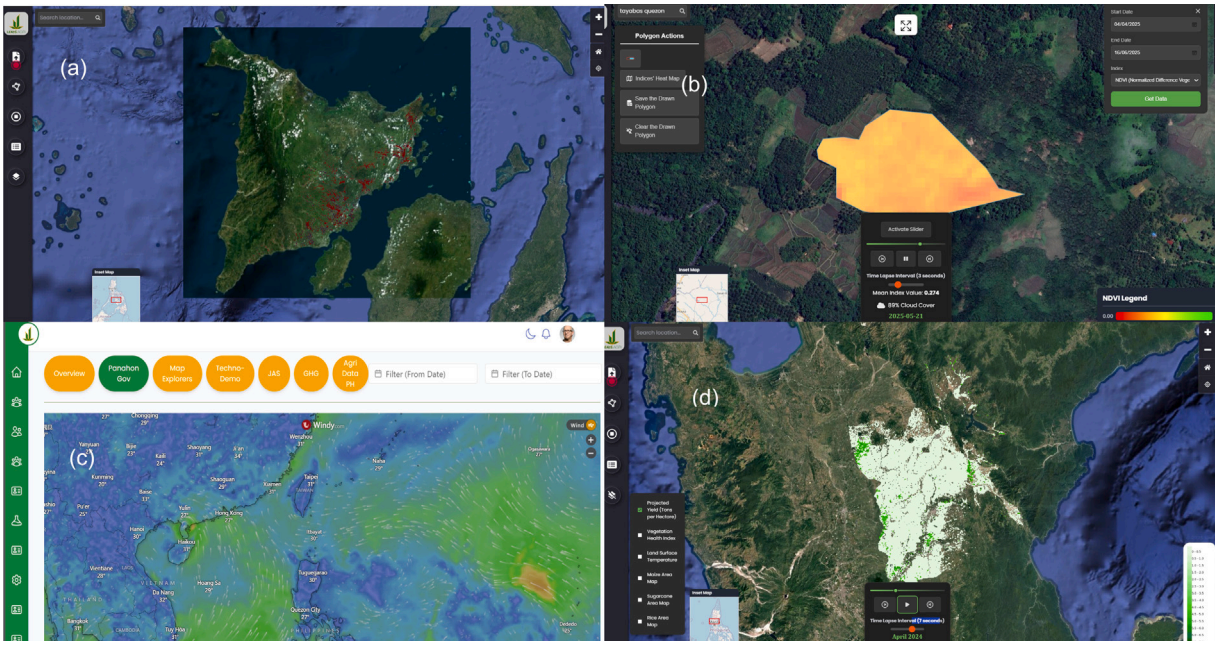

Fig. S1. The interface of the Digisaka platform showing AI-derived forecast maps and functioning as a CIS: (1) Flood inundation of Typhoon Odette; (b) Sample farm-level agricultural drought indication from VHI; (c) embedded platform real-time weather forecasts and (d) forecasted monthly rice yield from Digisaka system.

Data availability

The data supporting this study are available upon reasonable request.

References

[1] T.R. Knutson, S.J. Camargo, J.C.L. Chan, K.A. Emanuel, C.H. Ho, J.P. Kossin, M. Mohapatra, M. Satoh, M. Sugi, K.J.E. Walsh, L. Wu, Tropical cyclones and climate change assessment: Part II: Projected changes in intensity, size, and impacts, Bull. Am. Meteorol. Soc. 101 (3) (2020) E303–E322, http://dx.doi.org/10.1175/BAMS-D-18-0194.1.

[2] Bündnis Entwicklung Hilft and Ruhr University Bochum - Institute for International Law of Peace and Armed Conflict (IFHV), World Risk Report 2023, Bündnis Entwicklung Hilft and IFHV, Berlin and Bochum, 2023.

[3] D. Eckstein, V. Künzel, L. Schäfer, Global climate risk index 2021: Who suffers most from extreme weather events? Long-term analysis: 2000–2019, 2021, URL: https://www.germanwatch.org/en/19777.

[4] Philippine Statistics Authority, Table 4.13.2: Damages due to Natural Extreme Events and Disasters by Economic Activity for Major Disasters, 2012–2022, Philippine Statistics Authority, Quezon City, Philippines, 2023, Environmental and Natural Resources Accounting (ENRA) Dataset, https://psa.gov.ph/statistics/national-accounts/environmental-natural-resources-accounting.

[5] E.R. Florano, Integrated loss and damage–climate change adaptation–disaster risk reduction framework, in: Resilience, Elsevier, 2018, pp. 317–326, http://dx.doi.org/10.1016/b978-0-12-811891-7.00026-8, URL: http://dx.doi.org/10.1016/B978-0-12-811891-7.00026-8.

[6] Philippine Statistics Authority, 2012 Census of Agriculture and Fisheries (CAF) Highlights: Philippines, Technical Report, Philippine Statistics Authority, Quezon City, Philippines, 2015, Based on the 2012 Census of Agriculture and Fisheries; published in 2015, URL: https://library.psa.gov.ph/cgi-bin/koha/opac-detail.pl?biblionumber=2101.

[7] J.M. Pulhin, M.A. Tapia, Vulnerability and sustainable development: Issues and challenges from the Philippines' agricultural and water sectors, in: Sustainable Development and Disaster Risk Reduction, Springer Japan, 2016, pp. 189–206, http://dx.doi.org/10.1007/978-4-431-55078-5_12.

[8] W. Verzani, P. Corpuz, Typhoon Haiyan Damage Summary, GAIN Report, United States Department of Agriculture, Foreign Agricultural Service (FAS), Global Agricultural Information Network (GAIN), Manila, Philippines, 2013, Approved by Philip Shull, Agricultural Counselor, URL: https://apps.fas.usda.gov/newgainapi/api/report/downloadreportbyfilename?filename=Typhoon+Haiyan+Damage+Summary_Manila_Philippines_12-4-2013.pdf.

[9] BusinessWorld, Agriculture damage in western visayas estimated at P265M, 2020, URL: https://www.bworldonline.com/editors-picks/2020/01/06/271792/agriculture-damage-in-western-visayas-estimated-at-p265m/. (Accessed 28 October 2025).

[10] ReliefWeb, Southeast Asia: Drought – 2019–2020 (GLIDE DR-2019-000113-PHL), 2019, https://reliefweb.int/disaster/dr-2019-000113-phl. (Accessed YYYY-MM-DD).

[11] World Bank Group, Reforming Agricultural Insurance in the Philippines: Technical Report and Recommendations, Technical Report, World Bank, Washington, DC, 2023, Figure 3 reports penetration of ˜36–45% in 2021, URL: https://documents.worldbank.org/en/publication/documents-reports/documentdetail/099011124112030709.

[12] Y. Higuchi, N. Fuwa, K. Kajisa, T. Sato, Y. Sawada, Disaster aid targeting and self-reporting bias: Natural experimental evidence from the Philippines, Sustainability 11 (3) (2019) 771, http://dx.doi.org/10.3390/su11030771.

[13] C.B. Mata, O.F. Balderama, L.A. Alejo, J.L.R. Bareng, S.A. Kantoush, Satellite-based flood inundation and damage assessment: A case study of Typhoon Ulysses in Cagayan Valley, Philippines, Environ. Challenges 7 (2022) 100513, http://dx.doi.org/10.21203/rs.3.rs-1774502/v1.

[14] R.D. Tumaneng, K.E.R. Morico, J.A. Principe, Remote sensing and google earth engine for rapid flood mapping and damage assessment: A case of typhoons goni (rolly) and vamco (ulysses), in: International Archives of the Photogrammetry, Remote Sensing and Spatial Information Sciences, in: ISPRS Archives, vol. XLVIII-4/W8-2023, 2024, pp. 445–452, http://dx.doi.org/10.5194/isprs-archives-XLVIII-4-W8-2023-445-2024.
[15] G.J. Perez, O. Enricuso, K. Manauis, M.A. Valete, Characterizing the drought development in the Philippines using multiple drought indices during the 2019 El Niño, ISPRS Ann. Photogramm. Remote. Sens. Spat. Inf. Sci. V-3–2022 (2022) 463–470, http://dx.doi.org/10.5194/isprs-annals-v-3-2022-463-2022, URL: http://dx.doi.org/10.5194/isprs-annals-V-3-2022-463-2022.
[16] O. Rojas, Next generation agricultural stress index system (ASIS) for agricultural drought monitoring, Remote. Sens. 13 (5) (2021) 959, http://dx.doi.org/10.3390/rs13050959.
[17] E. Eze, A. Girma, A.A. Zenebe, G. Zenebe, Feasible crop insurance indexes for drought risk management in northern ethiopia, Int. J. Disaster Risk Reduct. 47 (2020) 101544, http://dx.doi.org/10.1016/j.ijdrr.2020.101544.
[18] E. Eze, A. Girma, A. Zenebe, J.M. Kourouma, G. Zenebe, Exploring the possibilities of remote yield estimation using crop water requirements for area yield index insurance in a data-scarce dryland, J. Arid. Environ. 183 (2020) 104261, http://dx.doi.org/10.1016/j.jaridenv.2020.104261.
[19] J.B.L.C. Dumalag, K.L.S. Mariano, N.R. Cadiz, A.E. Retamar, J.C. Aceron, M.M. Felicen, M.C. Gelido, Augmenting the Philippines' dost-asti's potential flood extents mapping service with S-Band novasar-1 images, Int. Arch. Photogramm. Remote. Sens. Spat. Inf. Sci. XLVIII-4/W8-2023 (2024) 203–210, http://dx.doi.org/10.5194/isprs-archives-xlviii-4-w8-2023-203-2024, URL: http://dx.doi.org/10.5194/isprs-archives-XLVIII-4-W8-2023-203-2024.
[20] S. Boeke, M.J.C. van den Homberg, A. Teklesadik, J.L.D. Fabila, D. Riquet, M. Alimardani, Towards predicting rice loss due to typhoons in the Philippines, Int. Arch. Photogramm. Remote. Sens. Spat. Inf. Sci. XLII-4/W19 (2019) 63–70, http://dx.doi.org/10.5194/isprs-archives-xlii-4-w19-63-2019, URL: http://dx.doi.org/10.5194/isprs-archives-XLII-4-W19-63-2019.
[21] F. Lansigan, W. de los Santos, J. Coladilla, Agronomic impacts of climate variability on rice production in the Philippines, Agric. Ecosyst. Environ. 82 (1–3) (2000) 129–137, http://dx.doi.org/10.1016/s0167-8809(00)00222-x, URL: http://dx.doi.org/10.1016/S0167-8809(00)00222-X.
[22] M. Boschetti, A. Nelson, F. Nutini, G. Manfron, L. Busetto, M. Barbieri, A.G. Laborte, Rapid assessment of crop status: An application of MODIS and SAR data to rice areas in Leyte, Philippines affected by Typhoon Haiyan, Remote. Sens. 7 (6) (2015) 6535–6557, http://dx.doi.org/10.3390/rs70606535.
[23] Y. Kurihara, M. Miyamoto, R. Sunakawa, Flood direct damage assessment due to Typhoon Ulysses by satellite images, Int. J. Disaster Risk Reduct. 118 (2025) 105067, http://dx.doi.org/10.1016/j.ijdrr.2024.105067.
[24] M.E.T. Tupas, F. Roth, B. Bauer-Marschallinger, W. Wagner, An intercomparison of sentinel-1 based change detection algorithms for flood mapping in Luzon, Philippines, Remote. Sens. 15 (5) (2023) 1200, http://dx.doi.org/10.3390/rs15051200.
[25] M. Lagmay, B.A. Racoma, Lessons from tropical storms urduja and vinta disasters in the Philippines, Disaster Prev. Manag.: Int. J. 28 (2) (2019) 154–170.
[26] X. Xie, B. Xie, J. Cheng, Q. Chu, T. Dooling, A simple Monte Carlo method for estimating the chance of a cyclone impact, Nat. Hazards 107 (3) (2021) 2573–2582, http://dx.doi.org/10.1007/s11069-021-04505-2.
[27] J.J.V. Dida, A.B. Araza, G.T. Eduarte, A.G.A. Umali, P.L. Malabrigo, R.A. Razal, Towards nationwide mapping of bamboo resources in the Philippines: testing the pixel-based and fractional cover approaches, Int. J. Remote Sens. 42 (9) (2021) 3380–3404, http://dx.doi.org/10.1080/01431161.2020.1871099.
[28] Iloilo PPDO, Iloilo provincial annual profile, 2022, https://www.iloilo.gov.ph/en/iloilo-provincial-profile. (Accessed 30 May 2025).
[29] DA-RFO 6, DRRMU FPOMD, Final damage report on typhoon odette as of 3PM, 24 February 2022, 2022, Unpublished internal report, transmitted via email by DA6 DRRMU FPOMD da6.drrm@gmail.com, Accessed via official communication.
[30] DA-RFO 6, DRRMU FPOMD, Final damage report on effects of drought/dry spell as of 3PM, 7 June 2024, 2024, Unpublished internal report, transmitted via email by DA6 DRRMU FPOMD da6.drrm@gmail.com, Accessed via official communication.
[31] M.R. Mabalay, J. Raviz, E. Alosnos, M. Barbieri, E. Quicho, J.E.A. Bibar, M. Barroga, M. Coñado, P. Mabalot, J.R. Mirandilla, A. Arocena, J. Maloom, G. Bello, E. Cariño, G. de Mesa, N. Detoito, H. Gonzaga, N. Martin, M.P. Tejada, M.J. Vives, M. Lastimoso, D.K. Bumagat, H. Cayaban, M. Barroga, R. Bayot, A.M. Callejo, N.M. Paguirigan, M.A. Gutierrez, G.C. Romuga, F.G. Amanquiton, J. Gan, E.P. Banasihan, C.C. Guevarra, A. Rala, H. Yonson, M. Malonzo, G.B. Berja, C. Diaz, L.A. Tamani, R.G. Roces, S. Asilo, J. de Dios, T.D. Setiyono, F. Holecz, E.J. Quilang, A. Laborte, The Philippine rice information system (PRiSM): An operational monitoring and information system on rice, in: Remote Sensing of Agriculture and Land Cover/Land Use Changes in South and Southeast Asian Countries, Springer International Publishing, 2022, pp. 133–150, http://dx.doi.org/10.1007/978-3-030-92365-5_7.
[32] S. Cohen, B.G. Peter, A. Haag, D. Munasinghe, N. Moragoda, A. Narayanan, S. May, Sensitivity of remote sensing floodwater depth calculation to boundary filtering and digital elevation model selections, Remote. Sens. 14 (21) (2022) 5313, http://dx.doi.org/10.3390/rs14215313.
[33] R. Bokusheva, F. Kogan, I. Vitkovskaya, S. Conradt, M. Batyrbayeva, Satellite-based vegetation health indices as a criteria for insuring against drought-related yield losses, Agricult. Forest. Meterol. 220 (2016) 200–206, http://dx.doi.org/10.1016/j.agrformet.2015.12.066.
[34] R.M. de la Cruz, N.T. Olfindo, Jr., M.M. Felicen, N.J.B. Borlongan, J.K.L. Difuntorum, J.J.S. Marciano, Jr., Near-realtime flood detection from multi-temporal sentinel radar images using artificial intelligence, Int. Arch. Photogramm. Remote. Sens. Spat. Inf. Sci. XLIII-B3-2020 (2020) 1663–1670, http://dx.doi.org/10.5194/isprs-archives-xliii-b3-2020-1663-2020, URL: http://dx.doi.org/10.5194/isprs-archives-XLIII-B3-2020-1663-2020.
[35] F.N. Kogan, Application of vegetation index and brightness temperature for drought detection, Adv. Space Res. 15 (11) (1995) 91–100, http://dx.doi.org/10.1016/0273-1177(95)00079-T.
[36] L. Ji, A.J. Peters, Assessing vegetation response to drought in the northern great plains using vegetation and drought indices, Int. J. Remote Sens. 24 (23) (2003) 5095–5108, http://dx.doi.org/10.1016/S0034-4257(03)00174-3.
[37] B.B. Shrestha, T. Okazumi, M. Miyamoto, H. Sawano, Flood damage assessment in the Pampanga river basin of the Philippines, J. Flood Risk Manag. 9 (4) (2016) 355–369, http://dx.doi.org/10.1111/jfr3.12174.
[38] A.M. Lagmay, Nationwide operational assessment of hazards (NOAH). A responsive program for disaster risk reduction in the Philippines, Humanit. Technol. Surv. Singap.: RSIS Cent. NTS Stud. (2017) 16–19.
[39] B.B. Shrestha, A. Kawasaki, W.W. Zin, Development of flood damage functions for agricultural crops and their applicability in regions of Asia, J. Hydrol.: Reg. Stud. 36 (2021) 100872, http://dx.doi.org/10.1016/j.ejrh.2021.100872.
[40] A.M. Ismail, Flooding and submergence tolerance, in: Genomics and Breeding for Climate-Resilient Crops: Vol. 2 Target Traits, Springer, 2013, pp. 269–290.
[41] Y. Yu, Y. Meng, P. Chen, K. Cao, Submergence stress reduces the ability of rice to regulate recovery after disaster, Agronomy 14 (6) (2024) 1319.
[42] M.L. Delos Reyes, W. David, The effect of El Niño on rice production in the Philippines, Philipp. Agric. Sci. 92 (2) (2009) 170–185.
[43] J.E. Villa, A. Henry, F. Xie, R. Serraj, Hybrid rice performance in environments of increasing drought severity, Field Crop. Res. 125 (2012) 14–24, http://dx.doi.org/10.1016/j.fcr.2011.08.009.
[44] M. Haghighi, Large-scale mapping of flood using sentinel-1 radar remote sensing, Int. Arch. Photogramm. Remote. Sens. Spat. Inf. Sci. 43 (2022) 1097–1102.
[45] P. van Rutten, I. Benito Lazaro, S. Muis, A. Teklesadik, M. van den Homberg, Flood and rice damage mapping for tropical storm talas in Vietnam using sentinel-1 SAR data, Remote. Sens. 17 (13) (2025) 2171, http://dx.doi.org/10.3390/rs17132171.
[46] B.B. Shrestha, H. Sawano, M. Ohara, N. Nagumo, Rice-crops flood damage assessment in the Pampanga river basin of the Philippines, Adv. River Eng. 21 (2015) 497–502.
[47] P. Gautam, B. Lal, R. Raja, R. Tripathi, M. Shahid, M. Baig, C. Puree, S. Mohanty, A. Nayak, Effect of simulated flash flooding on rice and its recovery after flooding with nutrient management strategies, Ecol. Eng. 77 (2015) 250–256, http://dx.doi.org/10.1016/j.ecoleng.2015.01.033.
[48] B. Flyvbjerg, M.K. Skamris Holm, S.L. Buhl, Underestimating costs in public works projects: Error or Lie? Journal of the American Planning Association 68 (3) (2002) 279–295, http://dx.doi.org/10.1080/01944360208976273.

[49] J.J. Yu, X.S. Qin, O. Larsen, Joint Monte Carlo and possibilistic simulation for flood damage assessment, Stoch. Environ. Res. Risk Assess. 27 (3) (2012) 725–735, http://dx.doi.org/10.1007/s00477-012-0635-4.
[50] E.N. Mendoza, A.G. Toledo-Bruno, A.S. Olpenda, Local government unit capacity for disaster risk reduction and management: from disaster to resilience, Adv. Environ. Sci. 8 (2) (2016) 148–156.
[51] E. Blanc, E. Strobl, Assessing the impact of typhoons on rice production in the Philippines, J. Appl. Meteorol. Clim. 55 (4) (2016) 993–1007, http://dx.doi.org/10.1175/jamc-d-15-0214.1, URL: http://dx.doi.org/10.1175/JAMC-D-15-0214.1.
[52] J. Raviz, M.A. Gutierrez, A. Laborte, Willingness to pay (WTP) for area-based yield (ARBY) index insurance product, 2024.
[53] A.M.F. Lagmay, G. Bagtasa, D.F. Andal, F.D. Andal, J. Aldea, D.C. Bencito, K. Liporada, P.A. Delmendo, An impact-based flood forecasting system for citizen empowerment, 2024, http://dx.doi.org/10.22004/AG.ECON.348355, URL: https://ageconsearch.umn.edu/record/348355.
[54] G. Wee, L.C. Chang, F.J. Chang, M.Z. Mat Amin, A flood impact-based forecasting system by fuzzy inference techniques, J. Hydrol. 625 (2023) 130117, http://dx.doi.org/10.1016/j.jhydrol.2023.130117.
[55] H. Greatrex, J.W. Hansen, S. Garvin, R. Diro, S. Blakeley, Scaling up index insurance for smallholder farmers: Recent evidence and insights, CGIAR Res. Program Clim. Chang. Agric. Food Secur. (CCAFS) (2015).
[56] K.J. Wienhold, D. Li, W. Li, Z.N. Fang, Flood inundation and depth mapping using unmanned aerial vehicles combined with high-resolution multispectral imagery, Hydrology 10 (8) (2023) 158, http://dx.doi.org/10.3390/hydrology10080158.
[57] J. Teng, D.J. Penton, C. Ticehurst, A. Sengupta, A. Freebairn, S. Marvanek, J. Vaze, M. Gibbs, N. Streeton, F. Karim, S. Morton, A comprehensive assessment of floodwater depth estimation models in semiarid regions, Water Resour. Res. 58 (11) (2022) http://dx.doi.org/10.1029/2022WR032031, e2022WR032031.
[58] B. Arshad, R. Ogie, J. Barthelemy, B. Pradhan, N. Verstaevel, P. Perez, Computer vision and IoT-based sensors in flood monitoring and mapping: A systematic review, Sensors 19 (22) (2019) 5012, http://dx.doi.org/10.3390/s19225012.
[59] T.G. Farr, P.A. Rosen, E. Caro, R. Crippen, R. Duren, S. Hensley, M. Kobrick, M. Paller, E. Rodriguez, L. Roth, D. Seal, S. Shaffer, J. Shimada, J. Umland, M. Werner, M. Oskin, D. Burbank, D. Alsdorf, The shuttle radar topography mission, Rev. Geophys. 45 (2) (2007) RG2004, http://dx.doi.org/10.1029/2005RG000183.
[60] R. Crippen, S. Buckley, P. Agram, E. Belz, E. Gurrola, S. Hensley, M. Kobrick, M. Lavalle, J. Martin, M. Neumann, et al., NASADEM global elevation model: Methods and progress, Int. Arch. Photogramm. Remote. Sens. Spat. Inf. Sci. 41 (2016) 125–128.
[61] D. Yamazaki, D. Ikeshima, R. Tawatari, T. Yamaguchi, F. O'Loughlin, J.C. Neal, C.C. Sampson, S. Kanae, P.D. Bates, A high-accuracy map of global terrain elevations, Geophys. Res. Lett. 44 (11) (2017) 5844–5853.
[62] Y. Ho, T. Hengl, Global ensemble digital terrain model 30m (GEDTM30), 2025, http://dx.doi.org/10.5281/ZENODO.15689805, URL: https://zenodo.org/doi/10.5281/zenodo.15689805.